Optik - International Journal for Light and Electron Optics 193 (2019) 162974

Contents lists available at ScienceDirect

Optik

journal homepage: www.elsevier.com/locate/ijleo

Original research article

Hybrid CuS-PEOT:PSS counter electrode for quantum sensitized solar cell

Amr Hessein[a,b,*], Ahmed Abd El-Moneim[b]

[a] Department of Mathematical and Physical Engineering, Faculty of Engineering (Shoubra), Benha University, Cairo, 11614, Egypt
[b] Department of Materials Science and Engineering, Egypt-Japan University of Science and Technology, New Borg El Arab City, Alexandria, 21934, Egypt

ARTICLE INFO

Keywords:
QDSSCs
PEDOT:PSS
Copper sulfide
Counter electrode
Polysulfide electrolyte

ABSTRACT

An inorganic/organic hybrid composite of CuS nanoparticles (NPs) and poly(3,4-ethylenedioxythiophene) polystyrene sulfonate (PEDOT:PSS) was prepared via a facile mixing process. Counter electrodes (CEs) of quantum dot sensitized solar cells (QDSSCs) were prepared by coating the hybrid CuS-PEDOT:PSS composite on fluoride-doped tin oxide (FTO) substrates using simple drop-casting technique. The SEM micrographs of CuS-PEDOT:PSS CEs revealed three-dimensional surface morphology and homogeneous dispersion of CuS NPs on the PEDOT:PSS. The electrochemical measurements of the hybrid CEs showed high electrocatalytic activity towards polysulfide electrolyte resulted from embedding the catalytic active CuS NPs into the continuous PEDOT:PSS conducting matrix. The CdS-QDSSC fabricated with CuS- PEDOT:PSS CE exhibited an remarkable stable power conversion efficiency (PCE) of 1.04%, that is higher than that of Pt CE (0.48%) measured under one-sun illumination. The enhancements in the photovoltaic performance of QDSSCs fabricated with hybrid CEs are discussed based on the analysis of electrochemical results.

1. Introduction

The Quantum dots-sensitized solar cell (QDSSC) is very promising third generation photovoltaic that has been brought to the scientists' attention lately. The great attention about QDSSCs was stemmed from the unique optoelectronic properties of the semiconductor quantum dots (QDs) as well as its ease of fabrication and low production cost [1–4]. A typical QDSSC device comprises three main components, namely, a photoanode, a counter electrode (CE), and the electrolyte. The photoanode is usually constructed from a TiO_2 mesoporous layer coated on FTO substrate and sensitized with a narrow bandgap QDs such as CdS, CdSe, PbS, etc [5–8]. Upon solar light exposure, the photo-generated excitons in the QDs are fastly dissociated at the bandgaps offset of the QDs-TiO_2 interface. The photo-electrons are thus transferred from the TiO_2 conduction band to the external circuit through the front electrode. The oxidized QDs are restored to the original state by accepting electrons a polysulfide (S^{2-}/S_x^{2-}) electrolyte. The electrons are collected from the external circuit by means of the CE and used to regenerate the oxidized polysulfide ions in the electrolyte. As subsequent to the particle size shrinkage, QDs had showed a number of advantageous and novel optoelectronic properties as a result of the quantum confinement effect. The exceptional properties of QDs such as bandgap tunability, high extinction coefficient, high intrinsic dipole-moment, and capability of multiple exciton generation by single photon were used to predict a theoretical light- to

* Corresponding author at: Department of Mathematical and Physical Engineering, Faculty of Engineering (Shoubra), Benha University, Cairo, 11614, Egypt.
E-mail address: amr.ahmed@ejust.edu.eg (A. Hessein).

https://doi.org/10.1016/j.ijleo.2019.162974
Received 10 April 2019; Received in revised form 10 June 2019; Accepted 18 June 2019

power conversion efficiency (PCE) of QDSSCs. A theoretical PCE of 44% has been calculated for QDSSC, which is higher than the theoretical Schottky- Queisser limit of 32% for silicon solar cell [9].

Nonetheless, the practical PCE values for QDSSCs devices are still situated far below the theoretical predicted PCE value [10]. Besides factors as the loss of photogenerated electrons by recombination at QDs-TiO_2 interface, the dearth of the perfect CE has been stated to be a major issue for the QDSSC inferior performance [11]. In earlier researches, scientists used to fabricate QDSSC devices with noble metals thin films CEs (e.g. Pt and Au CEs). QDSSCs assembled devices noble metals CEs suffered from low PCEs along with poor stabilities. The chemical degradation of the QDSSC devices was attributed to the sulfur adsorption on Pt or Au CEs surface while the poor performance resulted from their low electrocatalytic activity toward the (S^{2-}/S_x^{2-}) electrolyte reduction [12]. Hence, alternatives CEs for Pt and Au should satisfy the necessity requirements of high electrochemical activity, long-term chemical stability low-cost major issue to achieve high performance QDSSCs. Different materials such as transition metal chalcogenides [13–20], carbonaceous materials [21–23], and conducting polymers [24,25], had been tested and reported as CEs in QDSSC applications. Compared to the different developed CEs, copper sulfides Cu_xS (x = 1.0 to 2.0), CEs showed a promising improvement in PCEs owing to its appreciable activity for the polysulfide (S^{2-}/S_x^{2-}) reduction [26]. High performance Cu_xS CEs are mostly prepared by either sulfidation of brass sheets [2,17], or by the direct formation of Cu_xS thin films on the FTO substrate via various deposition techniques such as chemical bath deposition [15], SILAR [13] and hydrothermal method [27]. In addition to the inadequacy of these methods for mass production, QDSSCs assembled with those Cu_xS CEs usually suffered instability problems and a fast deterioration in PCEs were obtained due to the corrosion of Cu_xS CE in the presence of the liquid polysulfide electrolyte [28].

As mentioned earlier, the conducting polymers (CPs) were among the potential materials reported CEs in electrochemical devices such as QDSSCs. That is because most of CPs has showed good intrinsic conductivity, environmental stability, and large electrochemical surface area [11]. The conjugated bonding system along the polymer backbone cause the high intrinsic conductivity of CPs. Various types of CPs has been tested and reported as CEs in QDSSCs such as polyaniline (PANI) [24,29], Polypyrol (PPY) [10], poly (3,4-ethylene-dioxythiophene):poly(styrenesulfonate) (PEDOT:PSS) [30], etc. Among the different types of CPs, PEDOT:PSS has been intensively studied because of its aqueous solubility, chemical stability, low cost, availability, in addition to the ease of preparation. However and according to previous reports, pure PEDOT:PSS CEs was stated to be less efficient than the Pt CE regarding electrocatalytic activity and usually exhibit a poor fill factor. The flatness of PEDOT:PSS structure along with the large size of the dopant PSS chains were the main reasons considered for the inferior electroactivity of PEDOT:PSS CE as they resulted in imperfect contact between PEDOT active sites and the electrolyte [31,32]. Incorporating with electrochemical active NPs is suggested to improve the surface texturing of CE to be more accessible for the electrolyte infiltration leading to improve its electroactivity. On the other hand, attaching NPs to the PEDOT:PSS will make use of its conducting matrix to enhance the CE conductivity, increase the adhesion of NPs with the substrate, and also protect them from the corrosive effect of the electrolyte.

Hence, This study has been devoted to fabricate a new hybrid composite comprises of the PEOT:PSS and the catalytic active CuS NPs. The CuS NPs acted as an effective catalyst for polysulfide ions reduction, while PEOT:PSS represented a continuous conductive matrix with high surface area those used for fast electrons shuttling. For the sake of enhancing the contact and integrity between the composite components, PVDF was added. The activity of the fabricated CEs was examined by means of electrochemical measurements, cyclic voltammetry (CV), impedance spectroscopy (EIS), and Tafel polarization. The CdS QDSSC device fabricated with the CuS-PEOT:PSS CE has showed a remarkable enhancement in the photovoltaic performance with improved stability that is overcame the devices used Pt and the plain PEOT:PSS CEs. The obtained results proved the successful combination and the synergistic between CuS NPs and PEOT:PSS for efficient hybrid CEs.

2. Experimental

2.1. Copper sulfide nanoparticles preparation

Copper sulfide nanoparticles were prepared from the reaction of aqueous solutions of copper (II) nitrate [$Cu(NO_3)_2{\cdot}3H_2O$] and sodium sulfide ($Na_2S{\cdot}9H_2O$) aqueous solutions in the presence of ethylene glycol (EG). In brief, 5 mmol of $Cu(NO_3)_2$ were dissolved in 100 ml H_2O and EG with a volume ratio of (1:1) by stirring at 60 °C until we get a clear blue solution. Under vigorous stirring, 50 ml H_2O containing 6 mmol of Na_2S was quickly added to the $Cu(NO_3)_2$ solution. A fast reaction between the two solutions occurred and a dark green of the copper sulfide particles were quickly formed. After one hour of constant stirring at 60 °C, the nanoparticles were collected and washed several times with distilled water and ethanol using centrifugation and dried overnight at 80 °C in electric drying oven.

2.2. Counter electrodes preparation

All CEs were fabricated on fluorine-doped tin oxide (FTO) substrates (TEC-15) with sheet resistivity 15 Ω/□. The FTO substrates were firstly ultrasonically cleaned using a detergent solution, water, and then ethanol for 15 min each and naturally dried. Prior to CEs fabrication, the received PEDOT.PSS solution was filtered using 0.45 μm PTFE syringe filter to rid off the agglomerated and non-dissolved particles. For fabricating CuS-PEDOT.PSS CE, a 50 mg of the as prepared CuS NPs was dispersed in 0.5 ml of H_2O by ultrasonic and the then well mixed with 0.5 ml of PEDOT.PSS aqueous solution (Clevios P v4071 from H.C. Starck GmbH, solid content 1.2%) using ultrasonic for 30 min. The hybrid CE was then fabricated by drop casting 20 μl of the mixture on 1 cm^2 of pre-cleaned FTO substrate and dried at 50 °C for 12 h. The area of the CE was defined by using adhesive tape. The CuS-PEDOT.PSS-PVDF CE was prepared exactly as the same procedure except, CuS NPs were firstly dispersed in 0.25 ml H_2O and 0.25 ml DMF that

containing 5 mg PVDF before mixing with the PEDOT.PSS solution.

For the sake of comparison, pure PEDOT.PSS and platinum (Pt) CEs were fabricated and tested in parallel with the CuS-PEDOT.PSS and CuS-PEDOT.PSS –PVDF CEs. Pure PEDOT.PSS CE was fabricated from a sonicated mixture of 0.5 ml of pure double distilled H_2O with 0.5 ml of PEDOT.PSS solution. The Pt CE was prepared by the thermal decomposition of hexachloroplatinic acid in isopropanol (5 mM) casted on an FTO substrate at 500 °C.

2.3. Photoanodes preparations

A mesoporous layer of TiO_2 P25 of 10.5 ± 0.2 μm thickness was coated by the doctor blade technique over TiO_2 dense blocking layer and sintered at 500 °C for 1 h [33]. The coating paste was prepared by mixing TiO_2 P25 and ethyl cellulose as a binder in terpineol [28]. The surfaces of the photoanodes were then further treated with 100 mM $TiCl_4$ aqueous solution at 70 °C for 30 min. All photoanodes were sensitized with CdS QDs using the successive ionic layer adsorption and reaction (SILAR) method. Briefly, the photoanode was immersed for 1 min in 0.2 M $Cd(NO_3)_2{\cdot}4H_2O$ in methanol as a cation source (Cd^{2+}) to be adsorbed on the TiO_2 layer. The photoanode was then rinsed with methanol to remove the excess Cd^{2+} cations. Then, the photoanode was immersed in a 0.2 M Na_2S (methanol:water 1:1) solution as the anion source (S^{2-}) for 1 min, which was followed by rinsing with methanol. This four-step procedure was considered as one SILAR cycle. All the photoanodes were sensitized with 10 CdS SILAR cycles and also passivated with a ZnS layer prepared with four SILAR cycles using 0.1 M cation and anion precursor concentrations.

2.4. QDSSC devices fabrication

The QDSSC devices were fabricated by assembling the prepared photoanodes and CEs into sandwich-type solar cells with Parafilm as a spacer between the two electrodes. A regenerative polysulfide electrolyte (S^{2-}/S_x^{2-}) composed of 1 M Na_2S, 1 M S, and 0.1 M KCl in distilled water was used to fill the space between the two electrodes. The active areas of all tested devices were defined at fixed value of 0.28 cm^2 by clamping a shadow mask to the solar cell surface using binder clips.

2.5. Measurements and characterization

The crystallinity of the prepared CuS NPs was investigated using X-ray powder diffractometer (LabX XRD-6100; Shimadzu) equipped with Cu Kα radiation source with wavelength (λ = 1.5418 Å). Transmission electron microscopy (TEM) images and EDX measurements of CuS NPs were obtained by field emission microscope (JEM-2100 F; JEOL) operating at 200 kV using samples deposited on carbon coated copper grids. The surface morphology of the fabricated CEs was characterized by bench-top SEM (JCM-6000 plus; JEOL). Raman scattering spectra were measured with a Raman microscope (RAMANtouch) using a laser wavelength of 532 nm as excitation source. UV–vis absorption spectra were recorded on spectrometer (U-4000; Hitachi) equipped with a diff ;use reflectance unit. Photovoltaic measurements were carried out under AM 1.5 standard conditions with 1 sun illumination intensity (100 mW/cm^2) using (CT50AAA; Photo Emission Tech.) solar cell testing system. Electrochemical measurements were performed using a potentiostat unit (VersaSTAT 4; Princeton Applied Research). The sample used for the electrochemical measurements was a symmetrical dummy cell fabricated from two identical CEs separated with a spacer and the polysulfide electrolyte between them.

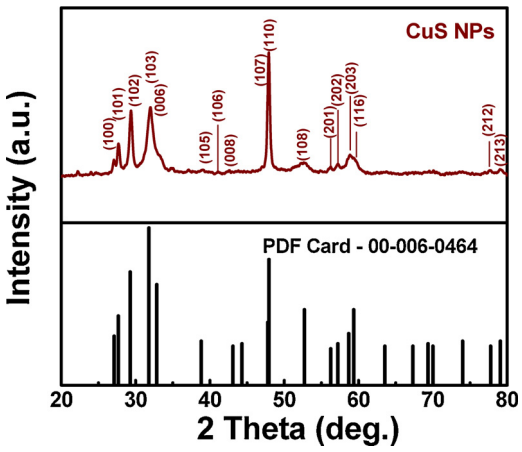

Fig. 1. XRD of the prepared CuS NPs.

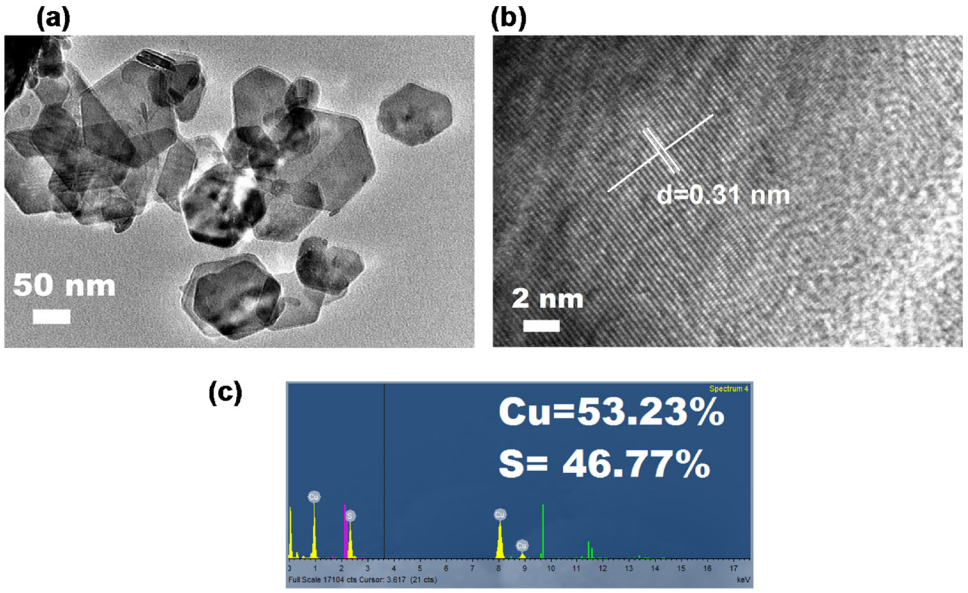

Fig. 2. (a) TEM, (b) HR-TEM, and (c) EDX of CuS NPs.

3. Results and discussion

3.1. Structure and morphology of the fabricated CEs

Fig. 1 shows the XRD pattern obtained for the prepared CuS NPs. All the diffraction peaks present in the diffraction pattern are well indexed to the covellite cupric sulfide phase (CuS) with hexagonal crystal structure, which well matched with the standard XRD pattern (JCPDS Card No. 00-006-0464). The pattern also clarifies the absence of any diffraction peak related to other non-stoichiometric Cu_xS phases.The slight broadening in CuS NPs diffraction peaks was the result of the small distortion in the lattice planes resulted from reducing the crystallite size to the nano size [34,35]. The average particle size of CuS NPs was estimated using Debby Scherrer's equation:

$$D = \frac{K\lambda}{\beta\cos\theta} \quad (1)$$

where K is a shape factor equal to 0.89, λ is the wavelength of the X-ray equal to 1.5406 Å, β is the full-width at half maximum (FWHM) in radians calculated from the diffraction peak intensity and θ is the Bragg's angle [36,37]. The average particle size was calculated to be about ˜ 56 nm based on the FWHM of the highest intensity (110) peak at Bragg's diffraction angle of 47.9°.

To further examine the detailed structure of the prepared CuS NPs, the TEM and EDX techniques were subsequently performed. Fig. 2(a) shows the TEM image obtained for the CuS NPs. It can be seen that, the CuS sample is composed of hexagonal shape nanoparticles with different particles sizes ranges from 40 to 120 nm. The HRTEM image of in Fig. 2(b) reveals the well resolved lattice fringes, demonstrating the highly crystallinity nature of the as-prepared CuS NPs. The interplanar spacing was measured to be about 0.31 nm, matching fairly well with the {102} planes of the hexagonal CuS covellite phase of (JCPDS Card No. 00-006-0464).

The initial concentration and molar ratio of the copper (Cu) and sulfur (S) precursors in the mixed solution play an important role in the formation of copper sulfide phases as reported by in Kim et al., [27]. For this reason, the higher concentration of Na_2S solution than $Cu(NO_3)_2$ solution was intentionally used in order to provide more sulfide S^{2-} ions in the mixed solution during the CuS NPs preparation. The excess S^{2-} ions are able to guarantee a complete reaction between all the presented Cu^{2+} ions and forming a nearly pure covellite CuS phase. This assumption has been tested with the EDX analysis which was used as semi-quantitatively measurement to estimate the chemical composition and atomic weight ratio of Cu and S in the prepared CuS NPs. The EDX spectrum of CuS NPs represented in Fig. 2(c) shows the atomic ration between Cu and S after elimination the contribution from the copper-coated carbon supporting TEM grid. According to EDX analysis, the ratio of S content is 46.77% while that of Cu is 53.23% in the total composition of CuS NPs. Hence, the hybrid CEs fabricated from the as-prepared CuS NPs are suggested to show high electrocatalytic activity whereas S-rich Cu_xS CEs (e.g. CuS and $Cu_{1.2}S$) are superior in performance than S- deficient ones (e.g. $Cu_{1.8}S$ and Cu_2S) [38].

Three polymer-based CEs, namely, PEDOT:PSS, CuS-PEDOT:PSS, and CuS-PEDOT:PSS-PVDF CEs were fabricated and tested for the purpose of comparison with the Pt CE. The addition of PVDF as water insoluble binder has been incorporated into the hybrid CuS-PEDOT:PSS CE to increase the adhesion of the CE material on the FTO substrate and also improve the contact and integrity between the electrode components. The SEM micrograph of PEDOT:PSS CE in Fig. 3(a) showed a very smooth and compact surface, which is undesirable surface for electrochemical reaction and for electrolyte diffusion. On the other hand, the SEM micrographs of the other fabricated CuS-PEDOT:PSS, and CuS-PEDOT:PSS-PVDF composite CEs, Fig. 3(b) and (c), respectively, revealed the formation of

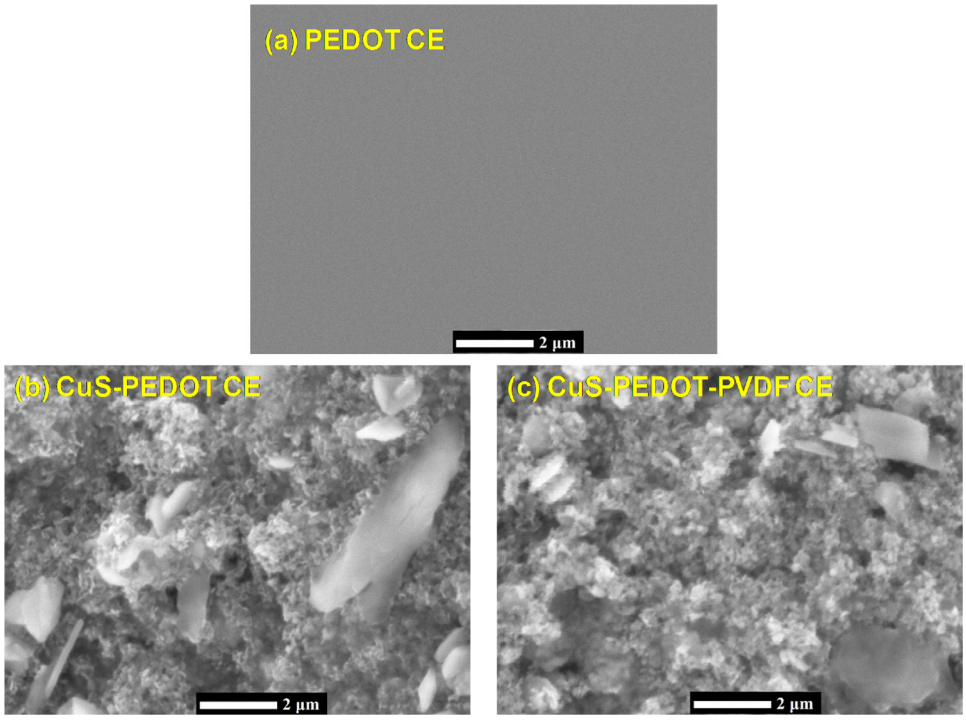

Fig. 3. SEM images of three PEDOT:PSS-based CEs.

three-dimensional (3D) porous structure. The micrographs also declare the uniform distribution of the CuS NPs through the PEDOT.PSS matrix. In principle, the 3D porous structure is often favorable for electrolyte infiltration into the structure of the developed CEs because it provides more reduction sites for efficient holes scavenging from the oxidized polysulfide ions. Finally, it is worth to note that there is no a clear differences in the apparent surface morphology of the hybrid composite CEs and the addition PVDF by small amount to CuS-PEDOT:PSS CE does not affect the porosity of the CE.

3.2. Electrochemical measurements

The role of the CE in QDSSC is collecting the electrons from the external circuit in addition to reducing the oxidized ions in the polysulfide electrolyte through electrons donation. Hence, the electrochemical activity of the fabricated CEs toward the polysulfide should be carefully investigated. In this regard, the electrochemical measurements: cyclic voltammetry (CV), electrochemical impedance spectroscopy (EIS), and Tafel polarization techniques were employed to evaluate the electrochemical performance and the reduction kinetics of the fabricated CEs. The electrochemical tests for the CEs were carried out in two electrode configuration on symmetrical cells (CE/electrolyte/CE) and the obtained results are shown in Fig. 4. The cyclic voltammograms of all the tested CEs were acquired at a scan rate of 100 mV.s^{-1} and given in Fig. 4(a). The negative reduction current density (J_{red}) in the CV was used to estimate the CEs catalytic activity toward the polysulfide electrolyte. It can be seen from Table 1, both hybrid CEs composed from CuS NPs and PEDOT:PSS recorded higher J_{red} values than the Pt and the bare PEDOT:PSS CEs suggesting their better activity. The high J_{red} ~ 13.2 mA/cm^2 obtained from CuS:PEDOT:PSS-PVDF CE compared to 8.79 mA/cm^2 obtained from the CuS:PEDOT:PSS CE. These obtained results clearly point out the role of PVDF addition in improving the adhesion of CE material to the FTO substrate which directly reflected on the catalytic performance of hybrid CE.

Fig. 4(b) and (c) show the measured EIS Nyquist plots for all fabricated CEs. The EIS data were recorded at zero bias voltage and 10 mV AC ramp amplitude in the frequency range from 0.1 Hz to 100 kHz. The EIS data were fitted to the equivalent circuit shown inset of Fig. 4(c) by Zsimpwin software and the calculated EIS parameters are summarized in Table 1. According to the used equivalent circuit, the series resistance (R_s) is given by the intercept of the EIS plot with the real axis and comprises the bulk resistance of the CE material and the sheet resistance of the supporting substrate [39]. R_{CT1} and the constant phase element (CPE1) are the charge transfer resistance and charging double layer capacitance at the solid-solid interface, whereas R_{CT2} and CPE2 are the charge transfer resistance and charging capacitance at the electrolyte-CE interface, respectively. Cleary Seeing from Table 1, a slight improvement in the R_s of the PEDOT:PSS CE from 41.3 Ω to 36.7 Ω upon mixing with CuS NPs has been observed. The lowest value of R_s ~ 25.4 Ω was obtained from the CuS-PEDOT:PSS-PVDF CE. The R_{CT1} that reached to 33.4 Ω achieved for the CuS-PEDOT:PSS-PVDF CE which far lower than 340 Ω and below 65.1 Ω of PEDOT:PSS and CuS-PEDOT:PSS CEs, respectively. Moreover, the very low of R_{CT2} values obtained from both hybrid CEs indicating high charge transfer kinetics at the CEs-electrolyte interface and favourable reduction of oxidized polysulfide ions at the CE surface. On the other side, the very high R_{CT2} values of the Pt and PEDOT:PSS CEs

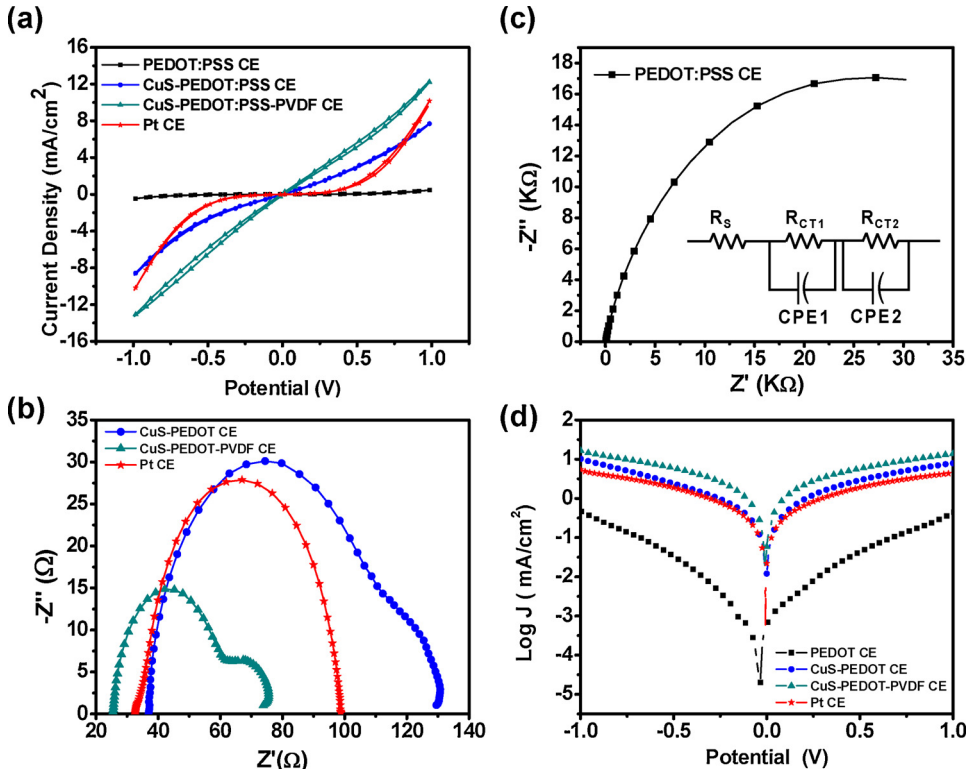

Fig. 4. (a) Cyclic voltammograms, (b) & (c) EIS Nyquist plots, and (d) Tafel polarization plots of the different CEs. The inset of (c) is the EIS equivalent circuit.

Table 1
Calculated electrochemical parameters for all tested CEs.

Counter Electrode	J_{red} (mA/cm^2)	J_{ex} (mA/cm^2)	J_{lim} (mA/cm^2)	R_s (Ω)	R_{CT1} (Ω)	R_{CT2} (Ω)
PEDOT:PSS CE	0.493	0.0013	0.467	41.3	340	41×10^3
CuS-PEDOT:PSS CE	8.79	1.25	10.16	36.7	65.1	21.3
CuS-PEDOT:PSS-PVDF CE	13.28	2.05	16.21	25.4	33.4	13.5
Pt CE	10.42	0.45	5.38	32.81	2.34	63.39

were resulted from their inferior activity toward the reduction of the polysulfide electrolyte.

Another beneficial electrochemical technique used to evaluate the capability of the fabricated CEs in catalyzing the reduction of polysulfide, is Tafel polarization measurements [40]. Fig. 4(d) shows the Tafel plots of the CE symmetric cells measured at scan rate 10 mV/s. The electrochemical activity of CEs can be evaluated for Tafel plot by means of the exchange current density (J_{ex}) determined from the intercept of the extrapolated linear region of the cathodic and anodic branches. J_{ex} is inversely related to charge transfer resistance (R_{CT}) according to the following equation:

$$J_{ex} = \frac{RT}{nFR_{CT}}, \tag{2}$$

where R is the universal gas constant, T is the temperature, n is the number of the electrons, and F is Faraday's constant. Thus, the higher electrochemical activity of the CE; is the higher J_{ex} and better charge transfer kinetics. The CuS-PEDOT:PSS-PVDF CE attained the highest J_{ex} of about 2.05 mA/cm^2, indicating its excellent catalytic activity than the other tested CEs. That is in a good agreement with the data obtained from the EIS measurements.

Furthermore, the limiting current density ($J_{\lim}$) of Tafel measurement is also used to evaluate the CE electrocatalytic activity. $J_{\lim}$ is determined from the intercept of the plot cathodic branch with the (log J) axis and it depends on the electrolyte diffusion coefficient (D) according to the relation:

$$D = \frac{l}{2nFC}J_{lim,} \tag{3}$$

where l is the spacer thickness, and C is the electrolyte concentration. The hybrid CEs were showed higher $J_{\lim}$ of 10.16 mA/cm^2 and

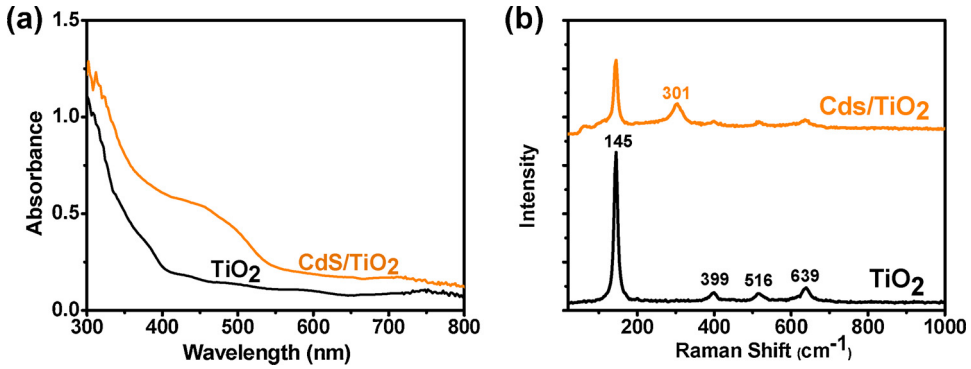

Fig. 5. (a) UV–vis absorption and (b) Raman scattering spectra of TiO_2 photoanode before and after sensitization with CdS QDs.

16.21 mA/cm^2, respectively, those are much higher than 0.46 mA/cm^2 for the bare PEDOT:PSS CE. The results are direct consequences of the 3D porous structure for both hybrid CEs which gave more electrolyte diffusion accessibility into the CEs as discussed before for their SEM micrographs in Fig. 3. On the other side, J_{lim} equals 5.38 mA/cm^2 was obtained for Pt CE referred to its poor electrochemical activity and the low electrolyte diffusion due to its compact structure.

In brief, the remarkable electrochemical performance of the hybrid CEs toward $S^{2-}/S_x{}^2$ electrolyte was emerged for the combination between CuS NPs and PEDOT:PSS with their unique properties. The catalytic active CuS NPs were responsible for providing more active sites for catalyzing the reduction of oxidized polysulfide ions at the CE surface. The supporting PEDOT:PSS matrix on the other side introduced a large apparent surface area and conductive network for fast electrons shuttling and a rapid reduction process. Hence, by merging the two materials in single hybrid CE, an outstanding electrochemical performance in terms of high J_{red} and low charge transfer resistances compared to the bare PEDOT:PSS and the Pt CEs has been achieved. Moreover, the 3D porous structure has promoted more diffusion of the electrolyte into the hybrid CE which resulted in higher values for J_{ex} and J_{lim}. It is worth mentioning that the addition of PVDF to the hybrid CE has a further improvement on the electrochemical performance through introducing better adhesion between the hybrid composite active components and also with the FTO substrate. Therefore, the application of the hybrid CuS-PEDOT:PSS CEs for the QDSSC is expected to inhibit the photocarriers recombination loss at photoanode-electrolyte interface, and modify the TiO_2 Fermi level position to more negative potential with respect to polysulfide redox level [41]. Consequently, higher J_{SC}, V_{OC}, fill factor (FF), and PCE values for QDSSC devices are expected to be obtained.

3.3. Photovoltaic performance

The TiO_2 photoanodes used as working electrodes in QDSSC devices were sensitized by CdS QDs for 10 SILAR cycles. UV–vis and Raman techniques were used to monitor the effectiveness of sensitization process performed on the photoanodes. Fig. 5(a) shows the UV–vis of the TiO_2 photoanode before and after sensitization with CdS QDs. The spectrum of the bare TiO_2 electrode showed a low absorbance in the visible region with a clear absorbance knee around 400 nm that is corresponding to 3.1 eV bandgap for TiO_2 P25 nanoparticles. After the sensitization process, the overall photoanode absorbance has been increased within the entire visible region besides a red shift for the absorption knee to be around 550 nm. The broad absorption peak centered at 460 nm appeared in absorbance spectrum of TiO_2/CdS photoanode is due to the CdS QDs with average optical transition of 2.7 eV. From the Raman scattering measurements of the TiO_2/CdS photoanode shown in Fig. 5(b), a peak located at 301 cm^{-1} is superimposed on the bare TiO_2 electrode spectrum with the four well known Raman peaks (145, 399, 516, and 639 cm^{-1}) of TiO_2 anatase phase. The new Raman peak is corresponding to the fundamental longitudinal (LO) phonons vibration of the CdS QDs [42]. The results of the acquired spectroscopic measurements confirm the successful incorporation between CdS QDs of suitable visible absorption and the TiO_2 into the photoanode.

A schematic representation of the typical QDSSC structure assembled with hybrid CE and illustrating the charges transport pathway within the device is depicted in Fig. 6. The photoanodes with the structure FTO/TiO_2/CdS/ZnS were assembled into QDSSC devices with hybrid CuS-PEDOT:PSS NPs CEs and by using polysulfide electrolyte. In the current structure, the photo-generated electron is injected from CdS conduction band into the TiO_2 conduction band which in turn is directed to the external load via the FTO front electrode. The hole in CdS QDs is then filled by fast electron donation from the ($S^{2-}/S_x{}^{2-}$) redox electrolyte, while the oxidized polysulfide ions are reduced by accepting electrons from CuS NPs through a catalytic reaction. Herein, the continuous PEDOT:PSS matrix in the CE was used to improve the electrons transport from the external circuit to the CuS NPs for more faster reduction process and increase the conductivity of the CEs as well. Also, the wide bandgap ZnS coated over CdSe QDs was used as a passivation layer to suppress the recombination losses at photoanode-electrolyte interface.

The photovoltaic performances of the QDSSC devices assembled with the different CEs were measured under simulated solar light illumination at AM 1.5 G standard conditions with irradiance intensity of 100 mW/cm^2. The obtained photocurrent density-potential (*J–V*) characteristics are shown in Fig. 7(a), and the corresponding solar cell parameters, J_{SC}, V_{OC}, FF, and PCE are summarized in Table 2. It is clearly seen from the table, QDSSC devices fabricated with hybrid CEs have better performance than the devices assembled with the Pt and the bare PEDOT:PSS CEs. The QDSSC with the hybrid CuS-PEDOT:PSS CE showed a PCE of 0.68%, which

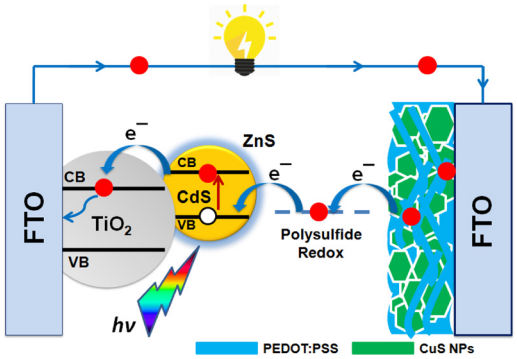

Fig. 6. Schematic representation of QDSSC assembled hybrid CuS- PEDOT:PSS CE.

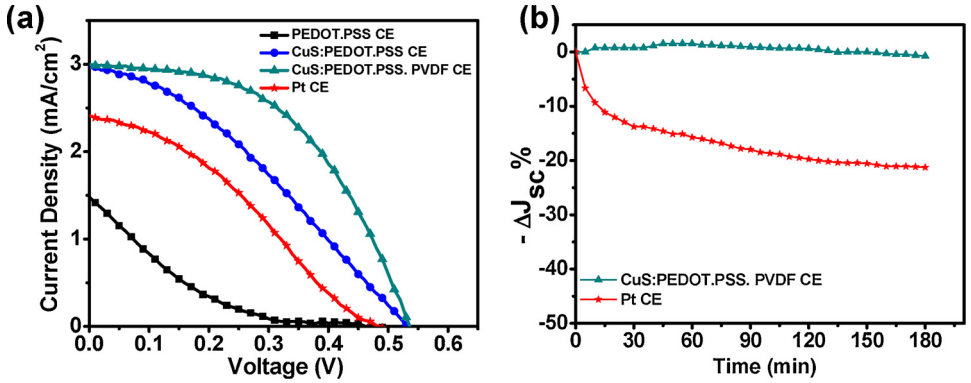

Fig. 7. (a) *J–V* characteristic curves of CdS QDSSCs based on the different CEs and (b) the photostability measurements.

Table 2
The Photovoltaic parameters for QDSSCs based on the different CEs obtained from the J–V curves in Fig. 7(a).

Counter Electrode	V_{OC} (V)	J_{SC} (mA/cm^2)	FF (%)	PCE (%)
PEDOT:PSS CE	0.464	1.47	12.0	0.11
CuS-PEDOT:PSS CE	0.533	2.96	33.0	0.68
CuS-PEDOT:PSS-PVDF CE	0.535	3.0	50.0	1.04
Pt CE	0.485	2.41	33.0	0.48

exceeds that is obtained from the cell with the Pt CE (0.48%). The high PCE obtained with CuS-PEDOT:PSS CE was also associated with high J_{SC} (2.96 mA/cm^2) and V_{OC} (0.533 V) values. These improvements in the photovoltaic performance are in consistent with the superior electrochemical activity of the hybrid CuS-PEDOT:PSS CE as revealed from the electrochemical measurements.

The photovoltaic performance of QDSSC was further enhanced by the addition of PVDF to the hybrid CE. The PCE of QDSSC with CuS-PEDOT:PSS-PVDF reached a value of 1.04%, much higher than the PCE values of the devices with both CuS-PEDOT:PSS and Pt CEs. This improvement can be only ascribed to the great enhancement in the FF from 33.0% with CuS-PEDOT:PSS CE to 50% for CuS-PEDOT:PSS-PVDF CE, since no significant improvement was observed in the J_{SC} and V_{OC}. The addition of PVDF to the hybrid CE has led to a remarkable decrease in the series and charge transfer resistances of the CE which facilitate the electrons transportation from the external circuit and fast reduction of S_x^{2-} ions. This gives rise to more efficient photoelectrons collection and also minimized the recombination loss at the photoanode-electrolyte interface pushing up the FF to a higher value and resulted in the good performance achieved.

In addition to the good photovoltaic performance, the QDSSC fabricated with CuS-PEDOT:PSS-PVDF CE showed a significant photostability compared to the device based on the Pt CE. The photostability measurements shown in Fig. 5(b) were performed by exposing the devices to continuous stimulated solar light for 3 h under normal ambient conditions while observing the change in J_{SC}. The device with Pt CE lost about 20% of the initial J_{SC} after 3 h of light soaking. On contrary, the device with the hybrid CE maintained its high performance with nearly 5% increase in the J_{SC} has been observed. The exhibited excellent photostability performance reveals the unique mechanical and chemical stability of the hybrid CE emerged from embedding CuS NPs within the chemically stable PEDOT:PSS matrix. The slight increase in J_{SC} may be attributed to deeper electrolyte infiltration within the hybrid CE by the effect of generated heating during the test.

4. Conclusions

In summary, An efficient, very stable, and cost-effective inorganic-organic hybrid CuS-PEDOT:PSS CE for QDSSC applications has been successfully synthesized. CuS NPs with pure covellite were prepared with facile low-temperature method which was confirmed by XRD and TEM measurements. A hybrid CuS-PEDOT:PSS composite was then prepared by liquid phase mixing and then directly coated on FTO substrate. The analysis of EIS, CV, and Tafel polarization measurements revealed a remarkable electrochemical performance of the hybrid CuS-PEDOT:PSS CEs that overcome the performances of Pt and plain PEDOT:PSS CEs. Further enhancement to the CE performance was also obtained by adding very small amount to the hybrid composite from PVDF, which also improved the CE mechanical properties. CdS-QDSSC fabricated with CuS-PEDOT:PSS-PVDF CE attained high photovoltaic performance and highly stable power conversion efficiency of 1.04%, that is much better than the devices fabricated with other CEs. The achieved results along with easy fabrication demonstrate the promising potential of our approach for inorganic/organic hybrid CE to replace the expensive and inefficient Pt CE for QDSSC applications.

Acknowledgements

The authors would like to express their sincere gratitude to the Egypt-Japan university of Science and Technology (E-JUST) and the Materials Science and Engineering (MSE) Department at E-JUST for their financial support in performing and finishing this work.

References

[1] J.G. Radich, R. Dwyer, P.V. Kamat, Cu2S Reduced Graphene Oxide Composite for High-Efficiency Quantum Dot Solar Cells.$^{2-}$ /S_n^{2-} at the Counter Electrode, J. Phys. Chem. Lett. 2 (2011) 2453–2460, https://doi.org/10.1021/jz201064k.
[2] W. Liang, L. Zhu, H. Liu, F. Xi, W. Li, CuS/brass based counter electrode in quantum dot-sensitized solar cells (QDSCs) with considerable efficiency and good stability, Electrochim. Acta 184 (2015) 285–294, https://doi.org/10.1016/j.electacta.2015.10.075.
[3] P.V. Kamat, Quantum dot solar cells. The next big thing in photovoltaics, J. Phys. Chem. Lett. 4 (2013) 908–918, https://doi.org/10.1021/jz400052e.
[4] N. Mir, A.A. Mir, P. Karimi, N. Poormolaei, Effect of chelating reagents on nanostructured CdS layer morphology in CdS-sensitized TiO_2 solar cells by successive ionic layer adsorption and reaction (SILAR) method, Mater. Sci. Semicond. Process. 77 (2018) 1–7, https://doi.org/10.1016/j.mssp.2018.01.006.
[5] Z. Chen, C. Wei, S. Li, X. Li, S. Dong, W. Zhang, CdS/CdSe co-sensitized hierarchical nanosheet-constructed NiO microballs for quantum-dot-sensitized solar cells, Optik (Stuttg). 172 (2018) 86–90, https://doi.org/10.1016/j.ijleo.2018.07.014.
[6] T. Lana-villarreal, J. Bisquert, CdSe quantum dot-sensitized TiO_2 electrodes : effect of quantum dot coverage and mode Ne, J. Phys. Chem. C. 113 (2009) 4208–4214.
[7] A. Badawi, N. Al-Hosiny, A. Merazga, A.M. Albaradi, S. Abdallah, H. Talaat, Study of the back recombination processes of PbS quantum dots sensitized solar cells, Superlattices Microstruct. 100 (2016) 694–702, https://doi.org/10.1016/j.spmi.2016.10.029.
[8] A. Hessein, A.A. El-moneim, Synthesis of copper sulfide/reduced graphene oxide nanocomposites for use as the counter electrodes of high-performance CdS-sensitized solar cells, New Carbon Mater. 33 (2018) 26–35, https://doi.org/10.1016/S1872-5805(18)60324-5.
[9] P.V. Kamat, Quantum dot solar cells. Semiconductor nanocrystals as light harvesters, J. Phys. Chem. C. 112 (2008) 18737–18753, https://doi.org/10.1021/jp806791s.
[10] M.H. Yeh, C.P. Lee, C.Y. Chou, L.Y. Lin, H.Y. Wei, C.W. Chu, R. Vittal, K.C. Ho, Conducting polymer-based counter electrode for a quantum-dot-sensitized solar cell (QDSSC) with a polysulfide electrolyte, Electrochim. Acta 57 (2011) 277–284, https://doi.org/10.1016/j.electacta.2011.03.097.
[11] I. Hwang, K. Yong, Counter electrodes for quantum-dot-Sensitized solar cells, ChemElectroChem. 2 (2015) 634–653, https://doi.org/10.1002/celc.201402405.
[12] K. Meng, G. Chen, K.R. Thampi, Metal chalcogenides as counter electrode materials in quantum dot sensitized solar cells: a perspective, J. Mater. Chem. A Mater. Energy Sustain. 3 (2015) 23074–23089, https://doi.org/10.1039/C5TA05071E.
[13] H. Salaramoli, E. Maleki, Z. Shariatinia, M. Ranjbar, CdS/CdSe quantum dots co-sensitized solar cells with Cu2S counter electrode prepared by SILAR, spray pyrolysis and Zn–Cu alloy methods, J. Photochem. Photobiol. A: Chem. 271 (2013) 56–64, https://doi.org/10.1016/j.jphotochem.2013.08.006.
[14] M. Eskandari, V. Ahmadi, R. Ghahary, Copper sulfide/lead sulfide as a highly catalytic counter electrode for zinc oxide nanorod based quantum dot solar cells, Electrochim. Acta 151 (2015) 393–398, https://doi.org/10.1016/j.electacta.2014.11.037.
[15] A.D. Savariraj, K.K. Viswanathan, K. Prabakar, CuS nano flakes and nano platelets as counter electrode for quantum dots sensitized solar cells, Electrochim. Acta 149 (2014) 364–369, https://doi.org/10.1016/j.electacta.2014.10.141.
[16] H. Geng, L. Zhu, W. Li, H. Liu, L. Quan, F. Xi, X. Su, FeS/nickel foam as stable and efficient counter electrode material for quantum dot sensitized solar cells, J. Power Sources 281 (2015) 204–210, https://doi.org/10.1016/j.jpowsour.2015.01.182.
[17] H. Zhang, H. Bao, X. Zhong, Highly efficient, stable and reproducible CdSe-sensitized solar cells using copper sulfide as counter electrodes, J. Mater. Chem. A Mater. Energy Sustain. 3 (2015) 6557–6564, https://doi.org/10.1039/C5TA00068H.
[18] M. Ye, X. Wen, N. Zhang, W. Guo, X. Liu, C. Lin, In situ growth of CuS and $Cu_{1.8}S$ nanosheet arrays as efficient counter electrodes for quantum dot-sensitized solar cells, J. Mater. Chem. A Mater. Energy Sustain. 3 (2015) 9595–9600, https://doi.org/10.1039/C5TA00390C.
[19] a.D. Mani, M. Deepa, P. Ghosal, C. Subrahmanyam, Novel single pot synthesis of metal (Pb, Cu, Co) sulfide nanomaterials -Towards a quest for paintable electrode materials that supersedes Pt electrode, Electrochim. Acta 139 (2014) 365–373, https://doi.org/10.1016/j.electacta.2014.07.009.
[20] C. Lin, C. Teng, T. Li, Y. Lee, H. Teng, Photoactive p-type PbS as a counter electrode for quantum dot-sensitized solar cells, J. Mater. Chem. A Mater. Energy Sustain. 1 (2013) 1155–1162, https://doi.org/10.1039/c2ta00251e.
[21] Q. Zhang, Y. Zhang, S. Huang, X. Huang, Y. Luo, Q. Meng, D. Li, Application of carbon counterelectrode on CdS quantum dot-sensitized solar cells (QDSSCs), Electrochem. commun. 12 (2010) 327–330, https://doi.org/10.1016/j.elecom.2009.12.032.
[22] G.S. Paul, J.H. Kim, M.S. Kim, K. Do, J. Ko, J.S. Yu, Different hierarchical nanostructured carbons as counter electrodes for Cds quantum dot solar cells, ACS Appl. Mater. Interfaces 4 (2012) 375–381, https://doi.org/10.1021/am201452s.
[23] J. Selvaraj, S. Gupta, S. Delacruz, V. Subramanian, Role of reduced graphene oxide in the critical components of a CdS-sensitized TiO_2-based photoelectrochemical cell, ChemPhysChem 15 (2014) 2010–2018, https://doi.org/10.1002/cphc.201402275.
[24] S. Abdulalmohsin, J. Armstrong, J.B. Cui, CdS nanocrystal-sensitized solar cells with polyaniline as counter electrode, J. Renew. Sustain. Energy 4 (2012) 043108, , https://doi.org/10.1063/1.4737133.
[25] X. Zhang, J. Zhang, Y. Cui, J. Feng, Y. Zhu, Carbon / polymer composite counter-electrode application in dye-sensitized solar cells, J. Appl. Polym. Sci. 5 (2013) 75–79, https://doi.org/10.1002/app.38147.
[26] Q. Shen, A. Yamada, S. Tamura, T. Toyoda, CdSe quantum dot-sensitized solar cell employing TiO_2 nanotube working-electrode and Cu_2S counter-electrode, Appl. Phys. Lett. 97 (2010) 10–13, https://doi.org/10.1063/1.3491245.
[27] S.S. Kalanur, S.Y. Chae, O.S. Joo, Transparent $Cu_{1.8}S$ and CuS thin films on FTO as efficient counter electrode for quantum dot solar cells, Electrochim. Acta 103 (2013) 91–95, https://doi.org/10.1016/j.electacta.2013.04.041.
[28] A. Hessein, F. Wang, H. Masai, K. Matsuda, A. Abd El-Moneim, One-step fabrication of copper sulfide nanoparticles decorated on graphene sheets as highly stable

and efficient counter electrode for CdS-sensitized solar cells, J. Appl. Phys. 55 (2016) 112301, , https://doi.org/10.7567/JJAP.55.112301.
[29] G. Yue, F. Tan, J. Wu, F. Li, J. Lin, M. Huang, W. Zhang, Cadmium selenide quantum dots solar cells featuring nickel sulfide/polyaniline as efficient counter electrode provide 4.15% efficiency, RSC Adv. 5 (2015) 42101–42108, https://doi.org/10.1039/C5RA02867A.
[30] T. Shu, X. Li, Z.L. Ku, S. Wang, S. Wu, X.H. Jin, C. Di Hu, Improved efficiency of CdS quantum dot sensitized solar cell with an organic redox couple and a polymer counter electrode, Electrochim. Acta 137 (2014) 700–704, https://doi.org/10.1016/j.electacta.2014.06.072.
[31] Y. Rhee, M. Ko, H. Jin, J.-H. Jin, N.K. Min, Photovoltaic performance of multi-wall carbon nanotube/PEDOT:PSS composite on the counter electrode of a dye-sensitized solar cell, J. Appl. Phys. 53 (2014) 08NJ02, , https://doi.org/10.7567/JJAP.53.08NJ02.
[32] P. Sudhagar, S. Nagarajan, Y.-G. Lee, D. Song, T. Son, W. Cho, M. Heo, K. Lee, J. Won, Y.S. Kang, Synergistic catalytic effect of a composite (CoS/PEDOT:PSS) counter electrode on triiodide reduction in dye-sensitized solar cells, ACS Appl. Mater. Interfaces 3 (2011) 1838–1843, https://doi.org/10.1021/am2003735.
[33] I. Barceló, J.M. Campiña, T. Lana-Villarreal, R. Gómez, A solid-state CdSe quantum dot sensitized solar cell based on a quaterthiophene as a hole transporting material, Phys. Chem. Chem. Phys. 14 (2012) 5801–5807, https://doi.org/10.1039/c2cp40609h.
[34] Y. Xie, L. Carbone, C. Nobile, V. Grillo, S. D'Agostino, F. Della Sala, C. Giannini, D. Altamura, C. Oelsner, X.C. Kryschi, P.D. Cozzoli, Metallic-like stoichiometric copper surface plasmon resonance properties, and their modeling, ACS Nano 7 (2013) 7352–7369, https://doi.org/10.1021/nn403035s.
[35] Y. Waseda, E. Matsubara, K. Shinoda, X-Ray Diffraction Crystallography, Springer Heidelberg, 2011, https://doi.org/10.1007/978-3-642-16635-8.
[36] M. Deng, Q. Zhang, S. Huang, D. Li, Y. Luo, Q. Shen, T. Toyoda, Q. Meng, Low-cost flexible nano-sulfide/carbon composite counter electrode for quantum-dot-sensitized solar cell, Nanoscale Res. Lett. 5 (2010) 986–990, https://doi.org/10.1007/s11671-010-9592-3.
[37] A. Tang, S. Qu, K. Li, Y. Hou, F. Teng, J. Cao, Y. Wang, Z. Wang, One-pot synthesis and self-assembly of colloidal copper(I) sulfide nanocrystals, Nanotechnology. 21 (2010) 285602, , https://doi.org/10.1088/0957-4484/21/28/285602.
[38] C.S. Kim, S.H. Choi, J.H. Bang, New insight into copper sulfide electrocatalysts for quantum dot-sensitized solar cells: composition-dependent electrocatalytic activity and stability, ACS Appl. Mater. Interfaces 6 (2014) 22078–22087, https://doi.org/10.1021/am505473d.
[39] A. Hessein, F. Wang, H. Masai, K. Matsuda, A.A. El-Moneim, Improving the stability of CdS quantum dot sensitized solar cell using highly efficient and porous CuS counter electrode, J. Renew. Sustain. Energy. 9 (2017) 23504, https://doi.org/10.1063/1.4978346.
[40] I.R.C. Rose, A.J. Rajendran, Exploring the effect of morphology of Ni and Co doped cadmium selenide nanoparticles as counter electrodes in dye-sensitized solar cell, Optik (Stuttg.) 155 (2018) 63–73, https://doi.org/10.1016/j.ijleo.2017.10.148.
[41] J.H. Zeng, D. Chen, Y.F. Wang, B. Bin Jin, Graphite powder film-supported Cu2S counter electrodes for quantum dot sensitized solar cells, J. Mater. Chem. C Mater. Opt. Electron. Devices 3 (2015) 12140–12148, https://doi.org/10.1039/C5TC02101D.
[42] A.G. Kontos, V. Likodimos, E. Vassalou, I. Kapogianni, Y.S. Raptis, C. Raptis, P. Falaras, Nanostructured titania films sensitized by quantum dot chalcogenides, Nanoscale Res. Lett. 6 (2011) 266, https://doi.org/10.1186/1556-276X-6-266.